A first-principles calculation of the magnetic moments and hyperfine parameters in amorphous Fe-B alloys

1990 J. Phys.: Condens. Matter 2 10559

(http://iopscience.iop.org/0953-8984/2/51/026)

J. Phys.: Condens. Matter 2 (1990) 10559–10572. Printed in the UK

A first-principles calculation of the magnetic moments and hyperfine parameters in amorphous Fe–B alloys

I Turek

Institute of Physical Metallurgy, Czechoslovak Academy of Sciences, Žižkova 22, CS-616 62 Brno, Czechoslovakia

Received 18 April 1990, in final form 2 October 1990

Abstract. The electronic structure of ferromagnetic amorphous alloys $Fe_{1-x}B_x$ ($0.14 \leqslant x \leqslant 0.23$) is calculated from first principles using the tight-binding linear muffin-tin orbital method in the atomic spheres approximation for realistic structural models. The concentration dependences of magnetization and average hyperfine parameters at iron nuclei (hyperfine magnetic fields and isomer shifts) are discussed with respect to the main mechanisms of their origin and to the structural characteristics of the atomic models used. The concentration behaviour of the magnetization is explained by means of the charge transfer from boron to iron which amounts to 0.75 electrons per boron atom and which is accompanied by a change in the shape of the density-of-states curves. It is shown that the composition dependence of the isomer shift is controlled by the interatomic charge transfer together with the intra-atomic s–d electron conversion. The behaviour of the hyperfine field can be explained by a core polarization proportional to the local magnetic moment of iron atom and by a valence contribution due to the s–d hybridization. The calculated values agree fairly well with existing experimental data.

1. Introduction

The magnetism of amorphous transition metal–metalloid (TM–M) alloys was studied by many workers during the last 15 years (for a review see, e.g., [1–3]). Of magnetic binary alloys with a metalloid content of 15–25 at.%, the $Fe_{1-x}B_x$ system has probably been the most explored. This alloy can be obtained by sputtering or coevaporating through a wide concentration range $0.1 \leqslant x \leqslant 0.9$ [4] and by liquid quenching in a limited interval $0.14 \leqslant x \leqslant 0.25$ [5] near the eutectic point at $x = 0.17$. Although the boron concentration accessible by melt quenching was recently increased up to $x = 0.35$ [6], the main physical and metallurgical interest remains confined to the vicinity of 17–20 at.% B, which is the common composition of many amorphous TM–M-based soft magnetic materials [1].

The basic magnetic property—the magnetization at zero temperature—has been studied experimentally by several methods, but very different results were obtained (for a review see [7]). The measured saturation magnetization exhibits a large scatter for amorphous samples of the same nominal composition; this is probably caused by the different histories of the samples. These discrepancies are most pronounced in the concentration dependence of the magnetic moment $m(x)$ per Fe atom. A linear decrease in $m(x)$ with x increasing between 0.12 and 0.25 was reported for rapidly quenched samples [8], but data suggesting more complicated dependences were also obtained

0953-8984/90/5110559 + 14 $03.50

[9, 10]. This ambiguity remains also in the case of sputtered samples [7]. A monotonic decrease in magnetization with increasing metalloid concentration was found for many other TM–M amorphous alloys [1]; however, a critical processing of experimental results of many workers showed that for the Fe–B system a parabolic dependence probably occurs with a maximum near $x = 0.17$ [7].

The compositional variation in the saturation magnetization of TM–M alloys is usually explained by means of the simple rigid-band model [1, 2]. This model assumes—apart from the constancy of the metal d band density of states (DOS) on alloying—that the majority spin subband is fully occupied and that the electron charge transfer from metalloid to metal atoms leads to the filling of the minority spin subband and to a reduction in the saturation magnetization [11]. As a consequence, this model predicts the charge transfer of about 1.5 electrons per boron atom in Fe–B alloys [2, 12], which would correspond to ionic character and seems to be rather unrealistic in metallic solids [2]. To clarify this question, realistic electronic structure calculations are desirable.

In addition to the macroscopic magnetization measurements, the type of chemical and topological short-range order present in TM–M alloys is currently studied by many microscopic experimental methods among which those based on hyperfine interactions (NMR and Mössbauer spectroscopy) are believed to provide information reflecting various local surroundings of absorbing nuclei [13]. However, wide distributions of hyperfine parameters at individual nuclei (hyperfine magnetic fields, isomer shifts (ISS) and electric field gradients) result in rather structureless absorption profiles and therefore the interpretation of the measured spectra for amorphous alloys is a difficult task even in the simplest binary alloys such as $Fe_{1-x}B_x$. Nevertheless, the average values of these distributions often exhibit easily measurable composition dependences which can be employed to study at least some connections between the amorphous structure and the measured data. The ^{57}Fe Mössbauer studies of the amorphous Fe–B system are ample (see, e.g., [4, 5, 14–16]) and will be discussed later.

On the other hand, there are only a few theoretical papers addressing the electronic structure of Fe–B amorphous alloys. Messmer [17] calculated charge densities and energy levels for a tetrahedral Fe_4B cluster using the spin-polarized SCF–X_α method and showed that considerable bonding interaction takes place between the central B atom and the corner Fe atoms. Fujiwara [18, 19] considered amorphous clusters containing about 1500 atoms with composition $Fe_{1-x}B_x$, $x = 0.15, 0.20, 0.25$. He performed first-principles tight-binding (TB) linear muffin-tin orbital (LMTO) calculations in the atomic spheres approximation (ASA) for the paramagnetic case and found the charge transfer from boron to iron of about 0.65 electrons per B atom [19]. Several workers used simple Harrison [20] parametrization of the TB Hamiltonian. Krompiewski *et al* [21] included the intra-atomic Coulomb repulsion into the parametrized paramagnetic Hamiltonian and obtained the main features of itinerant magnetism in amorphous $Fe_{1-x}B_x$, $0 \leqslant x \leqslant 0.6$. They arrived at the correct critical concentration $x_c = 0.6$ when the magnetization vanishes, and their $m(x)$ curve had a maximum for $x = 0.15$. Krajčí and Mrafko [22] studied the concentration dependence of the electronic structure for $Fe_{1-x}B_x$, $0.14 \leqslant x \leqslant 0.25$, and Krey *et al* [23] calculated the transport properties in the region $0.15 \leqslant x \leqslant 0.50$; both these studies were dealing with the spin–non-polarized case.

In this paper the electronic structure of ferromagnetic amorphous $Fe_{1-x}B_x$ alloys ($x = 0.14, 0.17, 0.20, 0.23$) is calculated by means of the TB LMTO ASA method and the recursion technique. To the present author's knowledge, the present study is the first where the electronic structure of the amorphous Fe–B system is numerically studied

from first principles in the ferromagnetic state. A detailed charge analysis is performed and the concentration behaviour of the saturation magnetization and average hyperfine parameters at Fe nuclei (hyperfine magnetic fields and ISs) is presented. In spite of some deficiencies in our approach (small cluster size and non-self-consistent calculation) the concentration dependences of the quantities studied are found to be in good agreement with existing experimental data. These trends are explained using the structural characteristics of our clusters and existing theoretical models.

2. Theoretical backgrounds and numerical calculations

2.1. Atomic structure modelling

The electronic structure calculations for amorphous clusters are usually performed with a certain model of atomic structure. A realistic model of the topological and chemical disorder present in an amorphous material is a necessary prerequisite for obtaining reasonable results. In this study, amorphous clusters with 100 atoms in a cube with periodic boundary conditions were used. The number of atoms was limited by our computer facilities while the particular boundary conditions were chosen to avoid surface effects. In this way, long-range order is artificially introduced into the structure, but experience shows that for our cluster size its influence on calculated quantities is negligible owing to strong topological disorder [24].

The modelling of the amorphous structure was based on interatomic pair potentials and the quasi-equilibrium atomic positions were obtained by the Markov-chain method [25], which is a special hybrid of the usual Monte Carlo and molecular dynamics techniques. Its essence lies in the prescription for the time evolution of the statistical assembly of atoms. The new atomic positions $\boldsymbol{r}_i'$ are derived from the old positions $\boldsymbol{r}_i$ using the expression

$$\boldsymbol{r}_i' = \boldsymbol{r}_i + \boldsymbol{v}_i\,\Delta t + \boldsymbol{F}_i(\Delta t)^2/2m_i \tag{1}$$

where $\boldsymbol{F}_i$ is the force acting on the ith nucleus, m_i is its mass and Δt is the time increment of the order of 10^{-14} s. The quantities $\boldsymbol{v}_i$ in (1) are random quantities the probability distribution of which has a Gaussian form with variance related to the temperature. As the interatomic potentials we took the truncated Morse potentials with the same parameters as in [26]. The density of the models was set to the experimental values for individual concentrations [9, 27].

The resulting pair distribution functions (PDFs) exhibit sharp Fe–Fe and Fe–B first coordination maxima and the often quoted B–B avoidance [28] (figure 1) (length is in atomic units (au) (Bohr radius), energy is in rydbergs (Ryd) and magnetic moments in Bohr magnetons (μ_B) throughout the paper). The second peaks in the Fe–Fe and Fe–B PDFs were not clearly split, probably owing to the modest cluster size. However, the parameter of Wendt and Abraham [29] (the ratio of the first minimum to the first maximum in the PDF) was lower than the critical value of 0.14 both for Fe–Fe and for Fe–B pairs, which indicates the glassy state. The average partial coordination numbers were also calculated and the results are presented in table 1. Their concentration dependences exhibit the monotonic trends observed experimentally, although the values

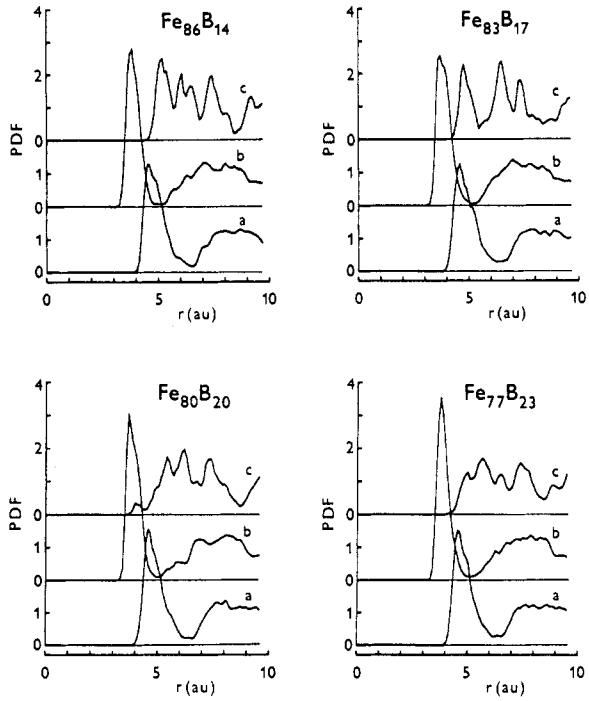

Figure 1. Distribution functions of Fe–Fe (curves a), Fe–B (curves b) and B–B (curves c) pairs of the four amorphous clusters.

Table 1. Densities and average partial coordination numbers for the structure models of $Fe_{1-x}B_x$.

x	ρ (g cm^{-3})	Z_{FeFe}	Z_{FeB}	Z_{BFe}
0.14	7.50	10.14	0.99	6.07
0.17	7.45	10.02	1.42	6.94
0.20	7.40	9.71	1.62	6.50
0.23	7.35	9.42	1.79	6.00

themselves are slightly lower [30]. Thus, we can conclude that our structural models represent a reasonable starting point for subsequent electronic structure calculations.

2.2. Electronic structure calculations

The recent first-principles TB LMTO ASA method of Andersen and coworkers [31–33] is well suited to real-space electronic structure calculations in disordered systems [19, 34, 35]. In our study, we used the simplest TB LMTO Hamiltonian

$$H_{RL,R'L'} = \bar{C}_{Rl}\delta_{RR'}\delta_{LL'} + (\bar{\Delta}_{Rl})^{1/2}\bar{S}_{RL,R'L'}(\bar{\Delta}_{R'l'})^{1/2} \tag{2}$$

where R and R' stand for the atomic positions (site index), and L and L' for the angular

momentum indices ($L = (l, m)$). The amorphous structure enters the Hamiltonian via the so-called screened structure constants matrix $\bar{S}_{RL,R'L'}$ while the scattering properties of individual atoms determine the potential parameters $\bar{C}_{Rl}$ and $\bar{\Delta}_{Rl}$. The potential parameters have a simple physical meaning: $\bar{C}_{Rl}$ and $\bar{\Delta}_{Rl}$ correspond essentially to the centre and the width, respectively, of the Rlth band. It should be noted that the Hamiltonian (2) yields the eigenvalues and eigenvectors correct to the first order in $E - E_{\nu Rl}$, where $E_{\nu Rl}$ are the energies chosen at the centre of the energy range of interest.

In densely packed structures, the matrix elements $\bar{S}_{RL,R'L'}$ are effectively zero if the interatomic distance $R - R'$ exceeds the distance of second-nearest neighbours and can be obtained from a Dyson-type matrix equation [32, 34]. To obtain the potential parameters, the radial Schrödinger equation within the atomic spheres must be numerically solved for the energy $E_{\nu Rl}$. The one-electron potential inside each atomic sphere should be calculated self-consistently. In the first approximation, however, we took the atomic potentials from [36, 37] for iron and boron atoms, respectively. Nine orbitals per iron atom (s, p, d) and four orbitals per boron atom (s, p) were used. The mutual shift of the iron and boron potentials was estimated from a preliminary electronic structure calculation for the orthorhombic Fe_3B. Apart from the splitting of the majority and minority spin bands of iron, our resulting potential parameters agree nicely with those calculated self-consistently in the case of paramagnetic $Fe_{80}B_{20}$ [35].

The large dimension of the Hamiltonian (2) prevented its direct diagonalization; instead, the recursion method was employed [38]. To calculate the total charges and magnetic moments of individual spheres together with the s, p and d components of these quantities, recursion coefficients were calculated for each RL orbital. Since the total number of orbitals was very large, only five recursion levels were obtained. The terminator—a delicate point with this small number of levels—was used in a Lorentzian form

$$t(E) = 1/(E - a + i\tfrac{3}{2}b) \tag{3}$$

where the constants a and b were determined from the chain parameters in the same way as for the usual square-root terminator [39]. We do not claim any universality of this terminator; however, the overall shape of the total DOS for $Fe_{80}B_{20}$ obtained with it agrees quite well with that calculated in our previous study [40] with 11 recursion levels and the square-root terminator. For another comparison, the total DOS per one spin for the pure non-magnetic amorphous iron is presented in figure 2. The resulting curve exhibits all substantial features reported in [19]. The two high peaks are of d character; the smaller peak at the bottom of the band is of s character. However, the heights of our d peaks are reversed in contrast with those in [19]. This disagreement is due to the small number of exact recursion levels. We believe that this inaccuracy in the DOS shape has no essential influence on the resulting integrated quantities (magnetic moments and hyperfine parameters).

From the DOSs, the magnetic moments were obtained as differences between the numbers of spin-up and spin-down electrons. This means that we dealt with the strictly ferromagnetic order with the exchange splitting given by that of crystalline iron and that we excluded the possibility of any other magnetic state. This highly simplified treatment is allowed in the composition region studied. A proper description of the iron-rich end down to pure amorphous iron should take into account the tendency to non-collinear ordering of local moments [1, 21].

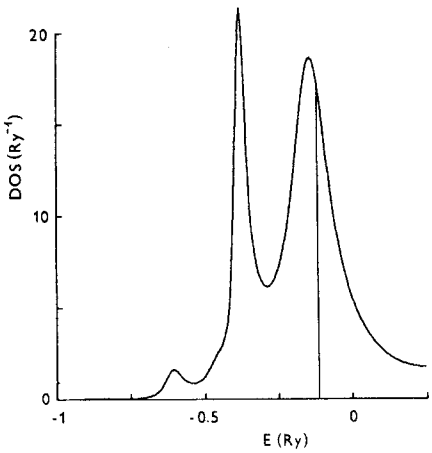

Figure 2. Total DOS per one spin for the pure non-magnetic amorphous iron. The vertical line denotes the Fermi energy.

Besides the magnetic moments, the valence electronic densities for both spin orientations can be calculated from the local DOSS. The formula for the valence charge density at a nucleus reads [32]

$$\rho_{R\sigma}(0) = (4\pi)^{-1} \int_{-\infty}^{E_F} g_{R\sigma}^{(s)}(E)[\Phi_{R\sigma}^{(s)}(0, E)]^2 \, dE \tag{4}$$

where R is the site index, σ is the spin orientation, E_F denotes the Fermi energy, $g_{R\sigma}^{(s)}(E)$ means the s-projected DOS for the Rth atom and spin σ, and $\Phi_{R\sigma}^{(s)}(r, E)$ is the solution of the radial Schrödinger equation for the s wave normalized to unity within the particular Wigner–Seitz sphere. In fact, a linearized version of equation (4) was used in the spirit of the LMTO theory [32].

The values of ISS are closely related to the electronic charge densities at the nuclei. The measured ISS correspond to very small relative changes in these densities of the order of 10^{-6}. The interpretation of ISS at Fe nuclei in metallic alloys is usually based on the idea of Ingalls [41] which states that the total density at a nucleus is the sum of a valence contribution from 4s-like electrons which depends mainly on the number of 4s electrons at the Fe atom and a core contribution due to 3s electrons which reflects, through the shielding effect, the number of 3d-like electrons at the Fe atom. However, recent *ab initio* calculations for dilute BCC iron alloys with substitutional impurities contradict these ideas [42] and show that the core electrons are of negligible importance for ISS and that the only relevant quantity is the number of valence s electrons. Thus, in the calculations of the IS presented in this work, only the valence density changes were considered. The ISS at Fe nuclei were then calculated according to

$$\text{IS}_R = \alpha[\rho_R(0) - \rho_{\text{BCC}}(0)] \qquad \alpha = -0.25 \text{ mm s}^{-1} \text{ au}^3 \tag{5}$$

where $\rho_R(0) = \rho_{R\uparrow}(0) + \rho_{R\downarrow}(0)$ is the total charge density, $\rho_{\text{BCC}}(0)$ is the reference charge density calculated by the same method for the BCC iron and α is the IS calibration constant the value of which was taken from [43].

Our hyperfine field calculations were confined to the Fermi contact term proportional to the spin density at the nucleus. This quantity can again be decomposed into a valence contribution and a core contribution. It is a well known fact that the core contribution is proportional to the local magnetic moment of the Fe atom (or to its d component

which is nearly the same) [44–47] while the valence contribution roughly scales with the s component of this magnetic moment. In this paper the valence contributions were calculated directly and the core contributions were obtained from the iron atomic moments. The total hyperfine magnetic field together with both contributions was calculated according to

$$\begin{aligned} B_R^{\text{core}} &= -Am_R \qquad A = 13.7\mu_B^{-1}\ \text{T} \\ B_R^{\text{val}} &= \beta[\rho_{R\uparrow}(0) - \rho_{R\downarrow}(0)] \qquad \beta = \tfrac{2}{3}\mu_0\mu_B = 52.43\ \text{T au}^3 \\ B_R &= B_R^{\text{core}} + B_R^{\text{val}} \end{aligned} \tag{6}$$

where m_R denotes the local magnetic moment and the value of the proportionality constant A was taken from [45].

3. Results and discussion

The average local and total DOSs for both spin polarizations are plotted in figures 3 and 4. The Fe local DOS exhibits two characteristic peaks of bonding and anti-bonding d character and a small bulge of s character near −0.6 Ryd. The boron local DOS consists of two peaks: one near −0.7 Ryd of s character and the other of p character. It should be noted that the centres of the boron s and p bands are located at −0.65 Ryd and 0.55 Ryd, respectively. The appearance of the boron p states below the Fermi level is caused by the strong hybridization with Fe d states. The boron s band is hybridized too, as seen from the total s charge (table 2). This analysis and that for various non-crystalline clusters [17, 19, 35] as well as for crystalline orthorhombic and body-centred tetragonal Fe_3B [48] show very similar features of the Fe–B interaction. This leads to the conclusion that the chemical bonding between the constituents of these alloys is of the same nature irrespective of the details of the atomic configuration.

The effect of the alloying on the shape of the Fe local DOS is clearly visible (figure 3). The addition of boron leads to a lowering of the bonding 3d peak on account of the anti-bonding 3d peak and to the suppression of exchange splitting. In this way the anti-bonding 3d peak of the minority spin is continually filled with electrons and the Fe moment is reduced with increasing boron content (see later). The changes in the iron DOS are not negligible within the composition range studied and throw doubt on the applicability of the rigid-band model up to $x = 0.6$ as sometimes done [12].

Our local and total DOSs (figures 3 and 4) can yield some information on the role of electronic structure in stabilizing the amorphous state. It is seen that for $x = 0.17$ a shallow local minimum in the total DOS arises just at the Fermi level. The boron concentration $x = 0.17$ exhibits simultaneously the highest glass-forming ability [7]. However, the connection between these facts and the Nagel–Tauc [49, 50] criterion is not clear. First, the Nagel–Tauc theory is based on the nearly-free-electron description inapplicable to the TM–M alloys and, second, our minimum in the total DOS for $x = 0.17$ is due to the magnetic exchange splitting rather than to the amorphous structure alone. In the paramagnetic state, the Fermi energy always falls into the region of high DOSs [18, 19, 22, 23]. The high stability of all amorphous TM–M alloys can be better explained by the above-mentioned boron p–iron d hybridization, leading to the bonding states below the Fermi energy with a certain degree of covalency.

The detailed charge analysis for the four concentrations is presented in table 2. The total charges n_{Fe} and n_B and their composition trends support clearly the idea of charge

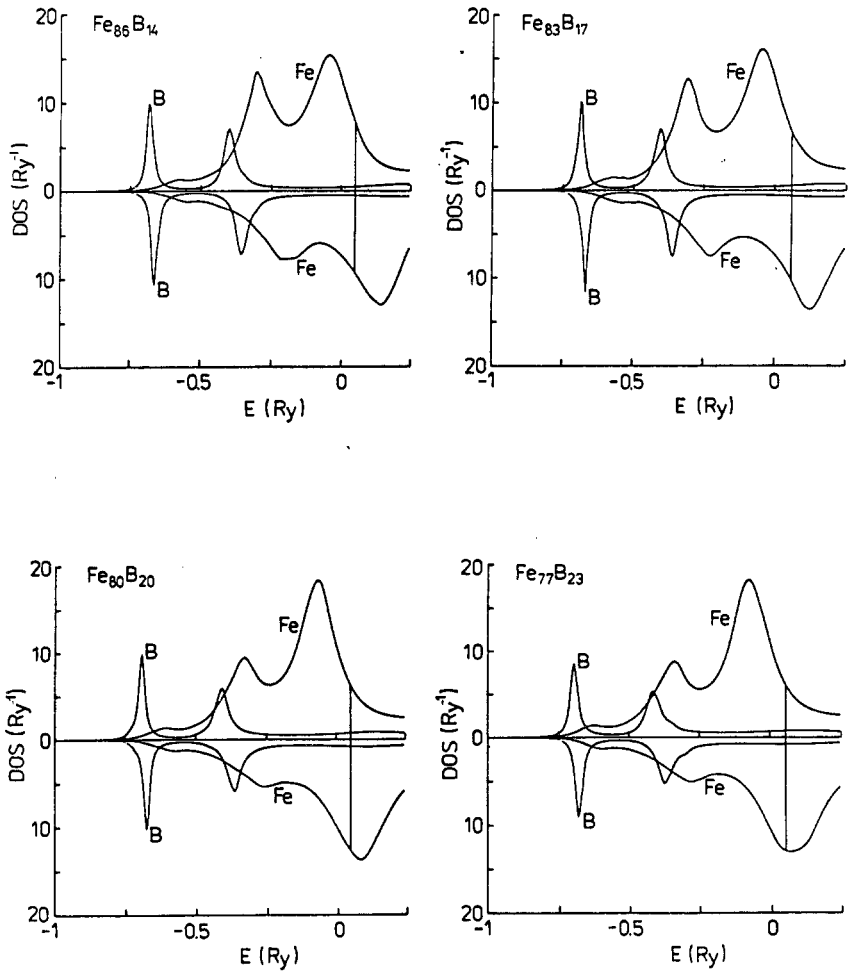

Figure 3. Local DOSS for iron and boron atoms for majority (upper curves) and minority (lower curves) spin. The vertical line denotes the Fermi energy.

transfer from boron to iron, this quantity being roughly 0.75 electrons per B atom. The resulting transfer is half the value of 1.5 electrons derived from Slater–Pauling curves assuming the rigid-band model [2, 12]. Our magnitude of the charge transfer can be compared with the self-consistent values of 0.98 [35] and 0.65 [19] electrons per B atom for paramagnetic $Fe_{80}B_{20}$. It should be noted that the exact quantity of charge transfer is highly sensitive to the mutual shift of the one-electron potentials of both components as well as to the choice of the Wigner–Seitz radii for the individual atoms. Our choice was $s_{Fe} = 2.699$ au, $s_B = 1.805$ au, while the values $s_{Fe} = 2.703$ au, $s_B = 1.907$ au were used in the quoted references.

As may be seen from the table 2, the total Fe charge increases and the charge transfer from B atoms decreases with increasing boron concentration, which may be interpreted in terms of increasing B coordination of Fe atoms (table 1). The concentration dependence of the partial charges reveals that it is mainly the d component of the Fe band

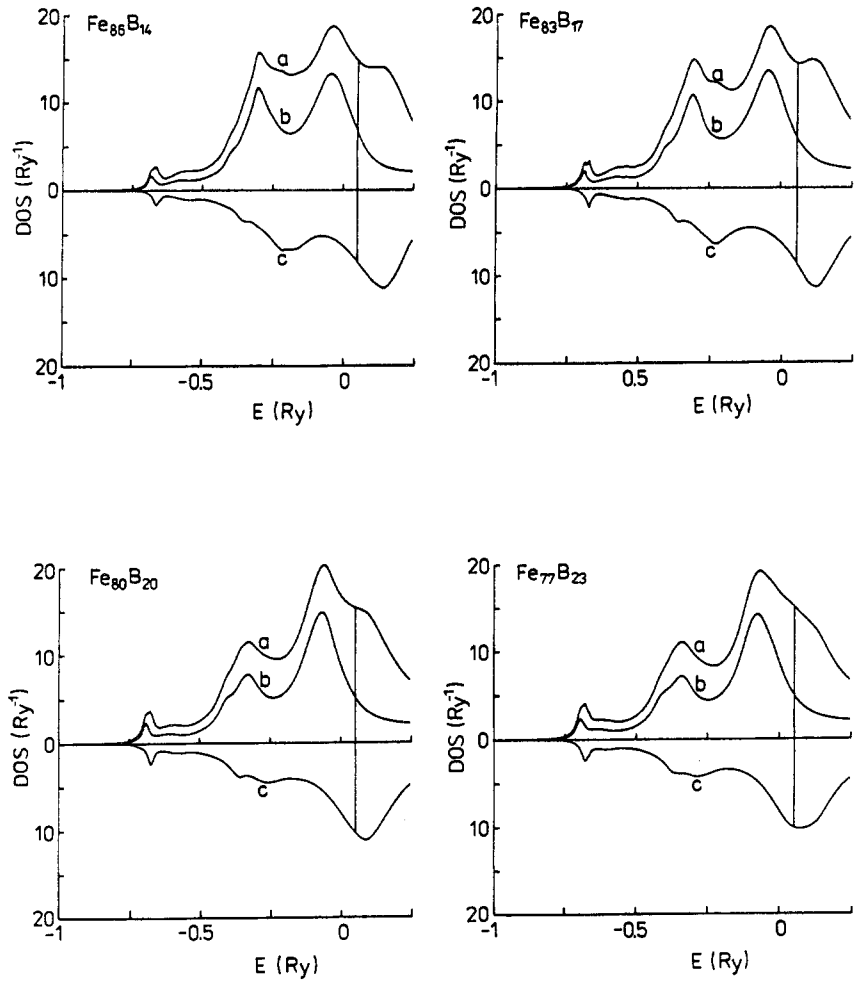

Figure 4. Total DOS (curves a) and its majority (curves b) and minority (curves c) components. The vertical line denotes the Fermi energy.

Table 2. Partial and total average charges of Fe and B atoms in $Fe_{1-x}B_x$.

	Charge						
x	Fe s	Fe p	Fe d	Fe total	B s	B p	B total
0.14	0.710	0.977	6.439	8.125	0.949	1.283	2.232
0.17	0.703	0.988	6.462	8.152	0.948	1.309	2.258
0.20	0.703	0.970	6.511	8.185	0.973	1.288	2.260
0.23	0.697	0.993	6.518	8.207	0.983	1.323	2.306

Table 3. Partial and total average magnetic moments of Fe and B atoms and magnetic moment m per Fe atom in $Fe_{1-x}B_x$.

	Magnetic moment (μ_B)							m
x	Fe s	Fe p	Fe d	Fe total	B s	B p	B total	(μ_B)
0.14	−0.015	−0.004	2.036	2.018	−0.027	−0.084	−0.110	2.000
0.17	−0.013	0.003	2.028	2.018	−0.027	−0.079	−0.106	1.996
0.20	−0.013	0.010	1.994	1.992	−0.026	−0.080	−0.107	1.965
0.23	−0.012	0.015	1.935	1.938	−0.027	−0.083	−0.109	1.905

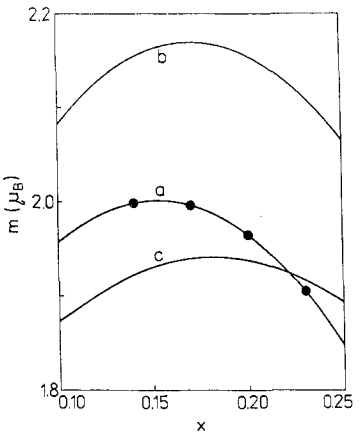

Figure 5. Magnetic moment m per Fe atom as a function of boron concentration in $Fe_{1-x}B_x$: ●, calculated values; curve a, parabolic fit of the calculated data; curve b, parabolic fit of the experimental data [7] for rapidly quenched samples; curve c, parabolic fit of the sputtered samples.

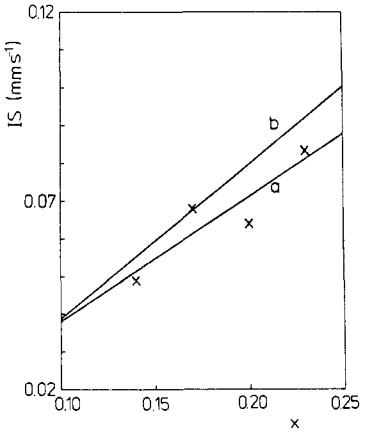

Figure 6. The calculated average ISS (×), their regression line (line a) and the line fitting experimental data [4] (line b).

which acquires the transferred electrons. This fact is in accord with existing ideas on this topic [1, 2].

The average magnetic moments of both constituents and their components are collected in table 3. Here, the magnetic moment per Fe atom is calculated according to

$$m = m_{Fe} + [x/(1-x)]m_B \tag{7}$$

which should be distinguished from the average magnetic moment of the iron atom itself due to the non-zero boron moment. The dependence $m(x)$ is plotted in figure 5 together with the least-squares parabolic fits of our results and of collected experimental results for both rapidly quenched and sputtered $Fe_{1-x}B_x$ [7]. It is seen that the parabola fits our data very well, leading to the maximum value of $2.00\mu_B$ for $x = 0.152$, while the other parabolae have their maxima at $x = 0.172$ and $x = 0.182$ for quenched and sputtered samples, respectively. The numerical studies of Krompiewski *et al* [21] also found the maximum to be at $x = 0.15$. On the basis of our calculations we can conclude that the

Table 4. Average ISs and average hyperfine fields at Fe nuclei together with their valence and core components in $Fe_{1-x}B_x$.

x	IS (mm s^{-1})	B^{core} (T)	B^{val} (T)	B (T)
0.14	0.049	−27.64	−4.13	−31.77
0.17	0.068	−27.65	−3.10	−30.74
0.20	0.064	−27.28	−3.03	−30.31
0.23	0.083	−26.54	−2.91	−29.45

non-monotonic dependence of $m(x)$ is due to the charge transfer and the change in the DOS shape on alloying.

While the iron moment varies on alloying, that of boron remains nearly constant and is of opposite sign. The latter is a common phenomenon found for light sp impurities in crystalline ferromagnetic hosts (see, e.g., [51, 52]) and is explained as a direct consequence of the hybridization between the impurity sp band and the host d band [51]. In our amorphous case the situation is similar since each B atom is surrounded only by Fe atoms.

The calculated average ISs at Fe nuclei are summarized in table 4 and in figure 6. The origin of the IS changes may be seen from table 2. Namely, the interatomic charge transfer from boron to iron is accompanied by an intra-atomic charge conversion of Fe s electrons into Fe d electrons which is manifested by the decrease in Fe s charge on alloying. Consequently, the resulting IS increases with increasing x in $Fe_{1-x}B_x$ alloys in agreement with experimental data (figure 6). The straight line fitting our calculated points gives the slope $\partial IS/\partial x = 0.331$ mm s^{-1} comparable with the experimental $\partial IS/\partial x = 0.42$ mm s^{-1} [4].

The measured concentration dependences of ISs in metallic alloys are often interpreted by means of the Miedema–van der Woude [53, 54] model. Their cellular atomic treatment supposes that three main mechanisms are responsible for the observed IS trends:

(i) an interatomic electron charge transfer due to different electronegativities of the alloy constituents;

(ii) an intra-atomic electron s–d transfer that equalizes the electron densities at the surfaces of individual Wigner–Seitz cells;

(iii) a physical contribution (a volume mismatch term) following from the atomic volume changes on alloying.

Analysing the experimental data for the $Fe_{1-x}B_x$ system in a large concentration range ($0.1 \leqslant x \leqslant 0.9$), Hoving *et al* [4] separated these individual contributions and showed that in the Fe-rich region the intra-atomic s–d transfer dominates. A similar result was obtained by Dubiel and Zinn [55] in their Mössbauer study of dilute BCC iron alloys. They concluded that for sp solutes (Al, Si, Sn and Ge) the s–d electron conversion is the most important process in the s electron redistribution. The present numerical results are in accordance with these conclusions.

It should be noted that our calculated ISs correspond to zero temperature while some of the Mössbauer experiments quoted were carried out at room temperature [4, 16] where the second-order Doppler shift is non-zero. However, as pointed out in [16] and

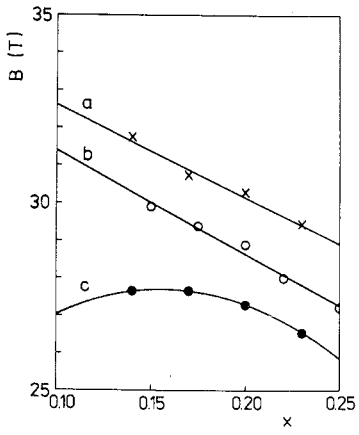

Figure 7. The calculated average hyperfine fields (×), their regression line (line a) and the experimental data (○) [15] together with their regression line (line b). The calculated core contributions (●) together with their regression parabola (curve c) are also plotted.

clearly shown in [5], the contribution of this quantity can be neglected provided that the line positions of the source and absorber are obtained at the same temperature.

The calculated average hyperfine magnetic fields and their contributions are presented in table 4 and figure 7 (the negative signs in table 4 denote the orientation of the hyperfine field with respect to the bulk magnetization and are omitted in figure 7 and in the following discussion). Contrary to the magnetization (figure 5), the total average hyperfine field is a monotonically decreasing function of the boron content. Experimental studies of this quantity (at zero temperature) revealed the same behaviour [5, 14, 15] irrespective of the preparation technique. These two differing composition dependences of magnetic quantities clearly show that the assumed proportionality between the magnetic moment and the total hyperfine field which is frequently used in interpretation of Mössbauer spectra should be employed with care [45]. In our study this proportionality was assumed for the core contribution only while the valence contribution was calculated independently. The values of the latter and of the s component of the iron magnetic moment are determined by the s–d hybridization for each spin orientation. As argued by Kaspar and Salahub [44] for disordered Fe–Co BCC alloys, this s–d hybridization is highly dependent on the environment of the atom and the magnitude of the valence contribution is positively correlated with the total magnetic moment of the nearest-neighbour shell. The same arguments probably remain true also in our case. With increasing iron concentration the first coordination shell contains more iron atoms and the polarization of the s-like electrons at the central Fe atom is more pronounced, which leads to a greater valence contribution.

To get a more quantitative comparison of the calculated hyperfine fields with zero-temperature measurements, the slopes of the concentration dependences $B(x)$ in the region of interest can be estimated: $\partial B/\partial x = -24.6$ T (our calculation) and $\partial B/\partial x = -27.6$ T (from [15]). The agreement is surprisingly good with respect to the approximations involved.

A comment should be made regarding frequent finite-temperature measurements of the hyperfine fields in Fe–B alloys (see, e.g., [5, 15, 16, 56]). The concentration dependence of the average hyperfine field is substantially modified on increasing temperature and becomes parabolic-like with a maximum near $x = 0.20$ at room temperature [15, 56]. This is due to the increase in the Curie temperature on alloying in the composition range studied [9]. This unpleasant fact throws serious doubt on simple interpretation of room-temperature measurements as presented, for example, in [16]. The

first-principles calculation of the finite-temperature behaviour of magnetic quantities in the sense of, for example, [57] is, however, a very difficult task and far beyond the scope of this paper.

4. Conclusions

The present study shows that the main experimental facts regarding the magnetization and the average hyperfine parameters at Fe nuclei in amorphous Fe–B in the concentration range 14–23 at.% B can be reproduced quite well even with the non-self-consistent first-principles calculation. The concentration dependence of the saturation magnetization can be—contrary to the rigid-band model—explained by simultaneous change in the iron DOS on alloying and a relatively small charge transfer from boron to iron. The chemical bond and the small magnetic moment of boron arises presumably owing to the Fe d and B sp hybridization. The difference between the concentration trends of magnetization per iron atom and the total hyperfine fields can be explained by s–d hybridization, leading to the important valence contribution to the hyperfine field. The charge analysis proves that besides the interatomic charge transfer from boron to iron an intra-atomic s–d electron conversion at Fe atoms occurs and controls the IS behaviour.

It seems that, in our approximate approach, mainly the chemical aspects of the problem were affected. It would be desirable to obtain some connection between the individual environment of a nucleus and the corresponding hyperfine parameters. Although it is not sure whether the resolution power of experimental hyperfine techniques will be able to extract more information than the average values and variances of the hyperfine distributions from an amorphous sample [13, 56], the present author believes that more detailed theoretical treatment can shed some light on this topic.

Acknowledgment

The author wishes to thank Dr M Šob for stimulating comments and helpful discussions as well as for critical reading of the manuscript.

References

[1] Handrich K and Kobe S 1980 *Amorphe Ferro- und Ferrimagnetika* (Berlin: Akademie)
[2] O'Handley R C 1983 *Amorphous Metallic Alloys* ed F E Luborsky (London: Butterworths) pp 257–82
[3] Lüscher E, Fritsch G and Jacucci G (ed) 1987 *Amorphous and Liquid Materials* (Dordrecht: Martinus Nijhoff)
[4] Hoving W, Scholte P M L O, Dorenbos P, Fokkema G A, Weits E A G, van der Woude F, Vincze I and Buschow K H J 1985 *Phys. Rev.* B **32** 8368
[5] Chien C L, Musser D, Gyorgy E M, Sherwood R C, Chen H S, Luborsky F E and Walter J L 1979 *Phys. Rev.* B **20** 283
[6] Nakajima T, Nagami I and Ino H 1986 *J. Mater. Sci. Lett.* **5** 60
[7] Cowlam N and Carr G E 1985 *J. Phys. F: Met. Phys.* **15** 1109
[8] Luborsky F E, Walter J L and Wohlfarth E P 1980 *J. Phys. F: Met. Phys.* **10** 959
[9] Hasegawa R and Ray R 1978 *J. Appl. Phys.* **49** 4174
[10] Hiroyoshi H, Fukamichi K, Kikuchi M, Hoshi A and Masumoto T 1978 *Phys. Lett.* **65A** 163
[11] Takács L 1979 *Phys. Status Solidi* a **56** 371

[12] Maksymowicz A Z, Stobiecki T, Jarocki E and Karas W 1984 *Phys. Status Solidi* b **126** 191
[13] Gonser U 1986 *Microscopic Methods in Metals* ed U Gonser (Berlin: Springer) pp 409–48
[14] Chien C L and Unruh K M 1982 *Phys. Rev.* B **25** 5790
[15] Dubois J M and Le Caer G 1982 *Nucl. Instrum. Methods* **199** 307
[16] Taniwaki M and Maeda M 1988 *Mater. Sci. Eng.* **99** 47
[17] Messmer R P 1983 *Amorphous Metallic Alloys* ed F E Luborsky (London: Butterworths) pp 114–25
[18] Fujiwara T 1982 *J. Phys. F: Met. Phys.* **12** 661
[19] Fujiwara T 1984 *J. Non-Cryst. Solids* **61–2** 1039
[20] Harrison W A 1980 *Electronic Structure and the Properties of Solids* (San Francisco: Freeman)
[21] Krompiewski S, Krey U and Ostermeier H 1987 *J. Magn. Magn. Mater.* **69** 117
[22] Krajčí M and Mrafko P 1988 *J. Phys. F: Met. Phys.* **18** 2137
[23] Krey U, Ostermeier H and Zweck J 1987 *Phys. Status Solidi* b **144** 203
[24] Jaswal S S 1985 *J. Non-Cryst. Solids* **75** 373
[25] Krajčí M and Mrafko P 1984 *J. Phys. F: Met. Phys.* **14** 1325
[26] Fujiwara T, Chen H S and Waseda Y 1981 *J. Phys. F: Met. Phys.* **11** 1327
[27] Waseda Y and Chen H S 1978 *Phys. Status Solidi* a **49** 387
[28] Nold E, Lamparter P, Olbrich H, Rainer-Harbach G and Steeb S 1981 *Z. Naturf.* a **36** 1032
[29] Wendt H R and Abraham F F 1978 *Phys. Rev. Lett.* **41** 1244
[30] Xianyu Z, Ishikawa Y, Fukunaga T and Watanabe N 1985 *J. Phys. F: Met. Phys.* **15** 1799
[31] Andersen O K and Jepsen O 1984 *Phys. Rev. Lett.* **53** 2571
[32] Andersen O K, Jepsen O and Glötzel D 1985 *Highlights of Condensed-Matter Theory* ed F Bassani, F Fumi and M P Tosi (Amsterdam: North-Holland) pp 59–176
[33] Andersen O K, Jepsen O and Šob M 1987 *Electronic Band Structure and Its Applications* ed M Yussouff (Berlin: Springer) pp 1–57
[34] Šob M, Jepsen O and Andersen O K 1988 *Z. Phys. Chem.* **157** 515
[35] Nowak H J, Andersen O K, Fujiwara T, Jepsen O and Vargas P 1990 in preparation
[36] Moruzzi V L, Janak J F and Williams A R 1978 *Calculated Electronic Properties of Metals* (New York: Pergamon) pp 168–73
[37] Herman F and Skillman S 1963 *Atomic Structure Calculations* (Englewood Cliffs, NJ: Prentice-Hall) pp 6–5, 6–6
[38] Haydock R 1980 *Solid State Physics* vol 35, ed H Ehrenreich, F Seitz and D Turnbull (New York: Academic) pp 215–94
[39] Beer N and Pettifor D 1984 *The Electronic Structure of Complex Systems* ed P Phariseau and W M Temmerman (New York: Plenum) pp 769–77
[40] Turek I 1986 *Proc. 16th Symp. on Electronic Structure* ed P Ziesche (Dresden: Technische Universität) pp 27–9
[41] Ingalls R 1967 *Phys. Rev.* **155** 157
[42] Akai H, Blügel S, Zeller R and Dederichs P H 1986 *Phys. Rev. Lett.* **56** 2407
[43] Ellis D E and Guenzburger D 1985 *Phys. Rev.* B **31** 1514
[44] Kaspar J and Salahub D R 1983 *J. Phys. F: Met. Phys.* **13** 311
[45] Sjörström J 1987 *Thesis* Uppsala University
[46] Blügel S, Akai H, Zeller R and Dederichs P H 1987 *Phys. Rev.* B **35** 3271
[47] Elzain M E and Yousif A A 1990 *Proc. Int. Conf. on the Applications of the Mössbauer Effect* at press
[48] Tegze M, de Groot R A, van der Woude F and Mueller F M 1985 *Rapidly Quenched Metals* ed S Steeb and H Warlimont (Amsterdam: North-Holland) pp 1031–4
[49] Nagel S R and Tauc J 1975 *Phys. Rev. Lett.* **35** 380
[50] Nagel S R 1982 *Adv. Chem. Phys.* **51** 227
[51] Akai H, Akai M, Blügel S, Zeller R and Dederichs P H 1984 *J. Magn. Magn. Mater.* **45** 291
[52] Šob M 1986 *J. Phys. F: Met. Phys.* **16** 577
[53] Miedema A R and van der Woude F 1980 *Physica* **100B** 145
[54] van der Woude F and Miedema A R 1981 *Solid State Commun.* **39** 1097
[55] Dubiel S M and Zinn W 1984 *Phys. Rev.* B **29** 2279
[56] Eibschütz M, Lines M E, Chen H S and Masumoto T 1984 *J. Phys. F: Met. Phys.* **14** 505
[57] Pindor A J, Staunton J, Stocks G M and Winter H 1983 *J. Phys. F: Met. Phys.* **13** 979